Eur. Phys. J. D (2017) 71: 25
DOI: 10.1140/epjd/e2016-70466-0

THE EUROPEAN PHYSICAL JOURNAL D

Regular Article

Dynamics of apokamp-type atmospheric pressure plasma jets

Eduard A. Sosnin[1,2,a], Victor A. Panarin[1], Victor S. Skakun[1], Evgeny Kh. Baksht[1], and Victor F. Tarasenko[1,2]

[1] Institute of High Current Electronics SB RAS, 634055 Tomsk, Russia
[2] Tomsk State University, 634050 Tomsk, Russia

Received 22 July 2016
Published online 9 February 2017 – © EDP Sciences, Società Italiana di Fisica, Springer-Verlag 2017

Abstract. The paper describes a new discharge source of atmospheric pressure plasma jets (APPJs) in air with no gas supply through the discharge region. In this discharge mode, plasma jets develop from the bending point of a bright current channel between two electrodes and are therefore termed an apokamp (from Greek 'off' and 'bend'). The apokamp can represent single plasma jets of length up 6 cm or several jets, and the temperature of such jets can range from more than 1000 °C at their base to 100–250 °C at their tip. Apokamps are formed at maximum applied voltage of positive polarity, provided that the second electrode is capacitively decoupled with ground. According to high-speed photography with time resolution from several nanoseconds to several tens of nanoseconds, the apokamp consists of a set of plasma bullets moving with a velocity of 100–220 km/s, which excludes the convective mechanism of plasma decay. Estimates on a 100-ns scale show that the near-electrode zones and the zones from which apokamps develop are close in temperature.

1 Introduction

Atmospheric pressure plasma jets (APPJs) have become a subject of much research interest due to their application in science and industry, including medicine, health care, materials processing, etc. [1–6]. Originally, the term APPJ denoted sources of nonthermal capacitively coupled plasmas produced by radio frequency excitation of gaseous media [5], and by now, there are many other methods of APPJ formation.

Generally, to produce APPJs, gas discharge plasma is created in a certain bounded volume and is expelled from this volume through a narrow capillary [1,3], a slit [7,8], or a set of holes [9] by excess pressure, which exceeds the atmospheric one, and by gas pumped through the discharge region.

Depending on the gas kind, discharge gap, and excitation mode, the initiating voltage can range from hundred volts to tens of kilovolts. Among the now available APPJ sources are those on helium and argon, nitrogen and air, and on mixtures of inert gases with nitrogen, oxygen, H_2O, CO_2, and other gases to provide desired concentrations of chemically active species in the plasma [1–14].

The atmospheric pressure plasma is excited by rf discharges [15,16], glow discharges [17–19], barrier discharges [7–11,13,14,20–24], and corona discharges [5,25,26], including various transition forms, e.g., microhollow cathode discharges [27,28] or sliding barrier discharges [29]. Each type of discharge used to produce APPJs is characterized by a certain range of parameters. For example, APPJs in a barrier discharge are produced by applying voltage pulses of positive and negative polarity, duration from several tens of nanoseconds to several microseconds, amplitude from hundred volts to tens of kilovolts, and repetition frequency of tens of kilohertz with a gas flow rate from several to tens of liters per minutes [20–23,30].

Our research in APPJs in air and nitrogen excited by high-voltage pulsed discharges has revealed a new phenomenon [24,31]: an extended plasma jet developing perpendicular to the bending point of the discharge channel between two electrodes. We named this discharge an apokamp (from Greek $\alpha\pi\acute{o}$ "off" and $\kappa\alpha\mu\pi\eta$ "bend"). It is found that the apokamp can represent a single needle or a conical jet of length 6–7 cm attached to the bending point of the current channel (Fig. 1). It should be noted that depending on the parameters of voltage pulses, the apokamp can also represent several plasma jets developing perpendicular to the current channel from the points of its bending.

High-speed recording demonstrates that APPJs, no matter what their type, are discrete and consist of numerous plasma bullets [32–42]. The data on plasma bullets in nitrogen and air are scanty. Some studies reported that the velocity of bullets in nitrogen was low and the jet front moved slowly [41]. In the pioneering study that demonstrated the possibility of bullets in an air jet [39], the bullet velocity was 1.25×10^2 km/s.

The apokamp phenomenon is new [31] and the apokamp dynamics is poorly understood. Here, we present high-speed photography data on the apokamp dynamics.

[a] e-mail: badik@loi.hcei.tsc.ru

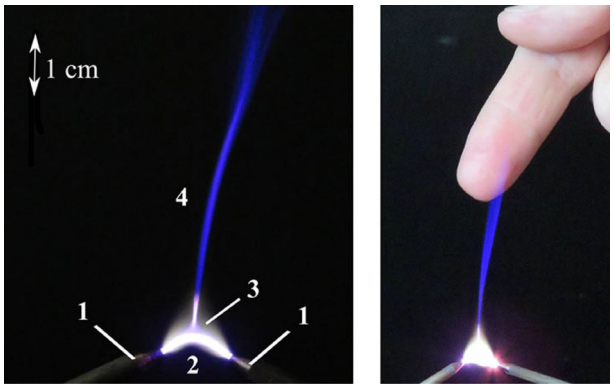

Fig. 1. Images of the phenomenon: *1* – sharp-ended electrodes; *2* – bending point of the current channel; *3* – halo; *4* – apokamp. The images were taken with a Canon PowerShot SX60 HS camera in frame-by-frame mode at ∼6.4 frm/s; in both cases, $f = 50$ kHz, $d = 1$ cm.

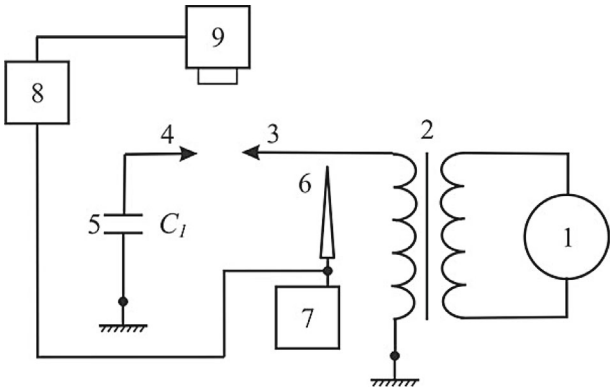

Fig. 2. Block diagram of the experimental setup: *1* – high-voltage generator; *2* – step-up transformer; *3* – high-voltage electrode of positive polarity; *4* – electrode capacitively decoupled with ground; *5* – capacitive decoupling ($C_1 = 10$ pF); *6* – high-voltage divider; *7* – oscilloscope; *8* – trigger generator for CCD camera; *9* – CCD camera.

We hope that the reported results can assist in developing a physical model of apokamps.

2 Experimental setup and measurements

A block diagram of the experimental setup is shown in Figure 2.

The voltage pulses produced by generator *1* were applied through step-up transformer *2* to high-voltage electrode *3*. As the voltage across electrode *3* was increased, a weakly glowing conical corona developed toward electrode *4*, not reaching the latter. After the discharge ignition, the gap between electrodes *3* and *4* was briefly closed and a current channel arose in the gap. Within two or three seconds, the channel became heated and a diffuse halo was formed around it (Fig. 1) due to convective displacement of the heated gas from the channel [42]. Almost immediately, the channel began to bend with the formation of a bright jet from the point of maximum bending; it is this phenomenon that we term an apokamp. Note that the formation of an apokamp required positive polarity of voltage pulses applied to electrode *3*.

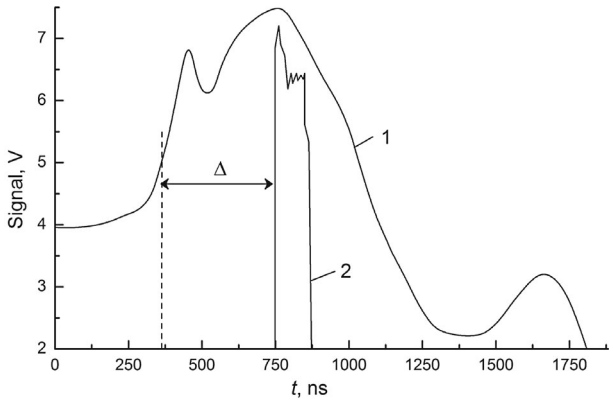

Fig. 3. Divider signal (*1*) and CCD camera trigger signal (*2*).

An important point is that the phenomenon is observed only when electrode *4* and ground are capacitively decoupled (C_1); with resistive coupling, no apokamp is formed. In idle mode, step-up transformer *2* produced output voltage pulses of positive polarity with a frequency of 16–96 kHz, duration of 1.5–2.5 μs, and amplitude of up to 23 kV. The pulses were applied to the electrodes of the discharge gap. To provide stable spatial location of an apokamp for high-speed photography, the electrodes were both made of steel and were both sharp ended, had a divergence angle of 120° (angle between them) and angle of the tip of 30°.

The apokamp dynamics was traced using an HSFC-PRO high-speed four-channel CCD camera with a minimum frame duration of 3 ns. For this purpose, CCD camera *9* (Fig. 2) was connected via trigger generator *8* (BNC 563, Berkeley Nucleonics Corp.) to high-voltage divider *6* (Tektronix P2100) spaced from electrode *3* by several centimeters. The signal from the divider was transmitted to oscilloscope *7*. Thus, we could control the trigger time of the camera with respect to the voltage pulse at the electrodes. Figure 3 illustrates the timing of the camera. The camera was triggered when the divider signal became higher than 5 V. Generator *8* also provided different delay times Δ for the CCD camera.

The APPJ spectrum was measured using a set of collimating lens with a focal length of 30 mm, optical fibers with a known bandwidth, and an Ocean Optics HR2000+ES spectrometer (not shown in Fig. 2) with a Sony ILX511B multichannel sensor (operating range 200–1100 nm, instrument function half-width ∼1.33 nm).

3 Results and discussion

The apokamp shape depends on the voltage amplitude, pulse frequency, and interelectrode gap d; in our experiments, $0.5 \leqslant d \leqslant 1.2$ cm. Thus, the apokamp can be shaped as a needle or a cone, or be straight or bent. Several plasma jets issuing from maximum bending points

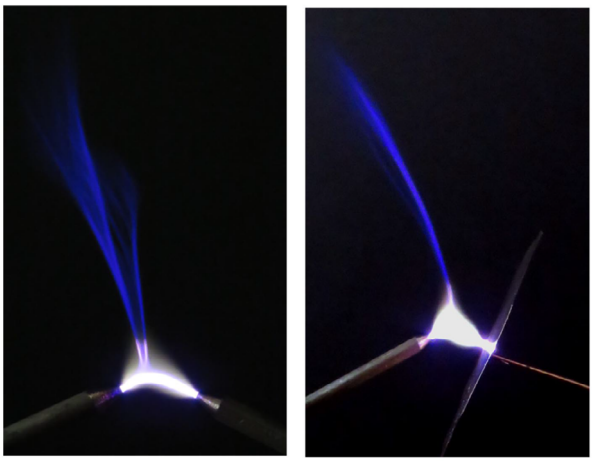

Fig. 4. Apokamp between a sharp-ended and a plane electrode (at the right) and between two sharp-ended electrodes (at the left) at $f = 50$ kHz and $d = 1$ cm; Canon PowerShot SX60 HS, frame-by-frame mode with ∼6.4 frm/s.

of the current channel are also possible (Fig. 4). The length and glow intensity of such jets are smaller than those of a single apokamp jet.

The apokamp could be tilted up to the horizontal line by varying the orientation of the electrode system. This suggests that the convective gas flow heated in the discharge channel little affects the formation of an apokamp.

The apokamp plasma temperature at the bending point of the current channel is rather high. Different materials were placed in the plasma at the bending point to detect their possible melting or ignition. In particular, we managed to melt a nichrome wire of diameter 0.1 mm. This means that at the bending point the average apokamp temperature was higher than 1100–1300 °C (melting temperature of nichrome). However, at the apokamp tip, the temperature was 100–250 °C such that the jet could be touched with a finger (Fig. 1). When the electrodes were placed in a bent tube with a hole, a stable plasma jet normally no longer than 1–1.5 cm was produced. The temperature at the jet tip decreased to 50 °C, allowing plasma treatment of temperature-sensitive materials. In particular, such apokamp jets were used for inactivation of *Staphylococcus aureus* and *Escherichia coli* [43].

Figure 5 shows typical oscillograms of the current and voltage across the electrodes for an apokamp. Interestingly, the voltage amplitude for the apokamp is 5–6% lower than that for the initial corona discharge, when the discharge gap between the electrodes is not closed (Fig. 2, electrodes *3* and *4*).

The radiation spectra of both the apokamp and the corona preceding the apokamp were typical for the plasma of a capillary barrier discharge in nitrogen [44], though the line intensity in the corona was 2–3 times lower than that in the apokamp. The spectrum was dominated by the second positive system of molecular nitrogen $N_2{}^*(C^3\Pi_u \rightarrow B^3\Pi_g)$ and relatively weak transitions of the first positive system N_2^+ $(B^2\Sigma_u^+ \rightarrow X^2\Sigma_g)$.

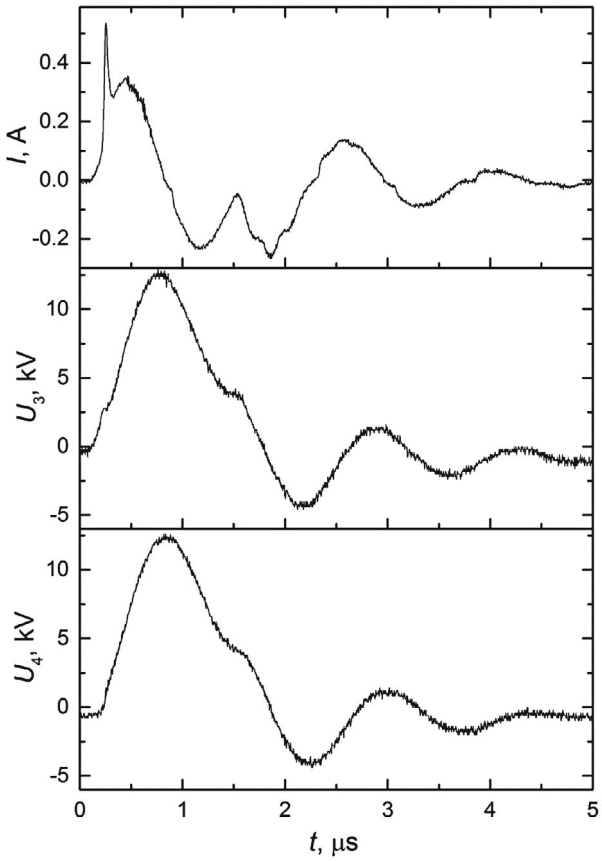

Fig. 5. Waveforms of the current and voltage U_3, U_4 across two sharp-ended electrodes at $d = 0.92$ cm.

In search for optimum trigger modes of the high-speed camera, it was found that apokamps were formed near the maximum of the gap voltage. The delay time was varied in the range 140 ns $< \Delta <$ 2.3 μs (Fig. 3), but the range in which an apokamp could be detected was narrow and was 340 ns $< \Delta <$ 380 ns. In all cases of high-speed photography, the electrodes were sharp ended, ensuring a high stability of the apokamp position and a high stability of recording.

Figure 6 shows the dynamics of a plasma bullet for a single jet. The first image corresponds to the stage before the process starts developing (Fig. 6a). Almost at the center of all other images, there is a bright spot of plasma formation (Figs. 6b–6d). It is seen that the spot and the bullet are formed at a time within the first 23 ns. The velocity of the bullet estimated from its frame-to-frame displacements is $v \sim 215$ km/s.

Figures 7 and 8 show the dynamics of plasma bullets for two and three plasma jets, respectively. The bullet velocity estimated from displacements of the central bullet in Figure 8 is $v \sim 215$ km/s. Other estimations give the velocity ranging from 100 to 220 km/s. This estimate is 10 times higher than those obtained for plasma bullets arising in helium and propagating in atmospheric pressure air [45]. Note that in our experiments, the gap voltage was also 10 times higher than that in the study cited [45]. At the same time, our estimate of v is an order of magnitude

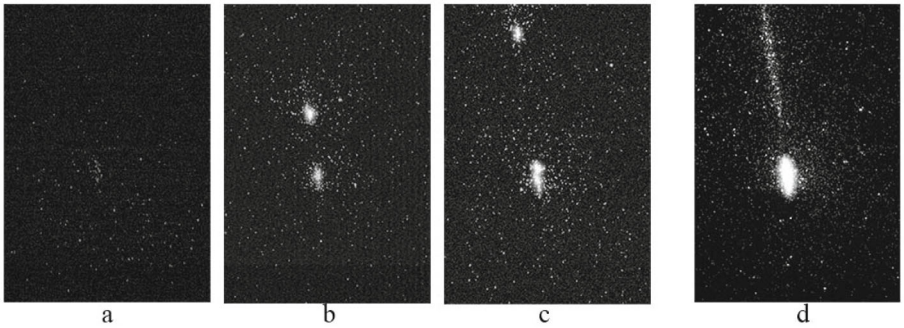

Fig. 6. Apokamp dynamics captured at an exposure of 3 ns and frame interval of 17 ns (a)–(c) and integral image at an exposure of 120 ns (d). The vertical frame size is 26.27 mm.

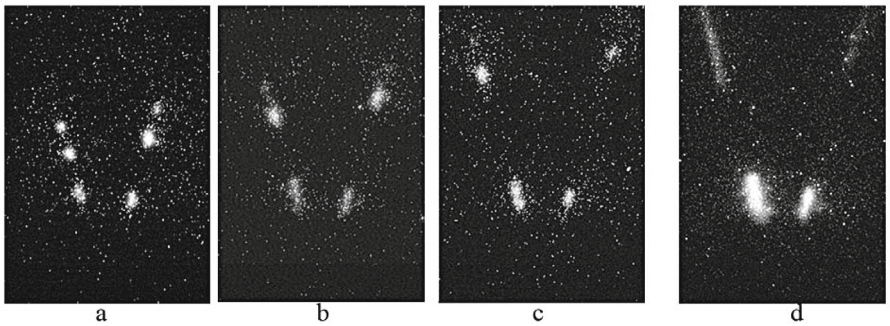

Fig. 7. Apokamp dynamics for two plasma jests captured at an exposure of 3 ns and frame interval of 17 ns (a)–(c) and integral image at an exposure of 120 ns (d). The vertical frame size is 26.27 mm.

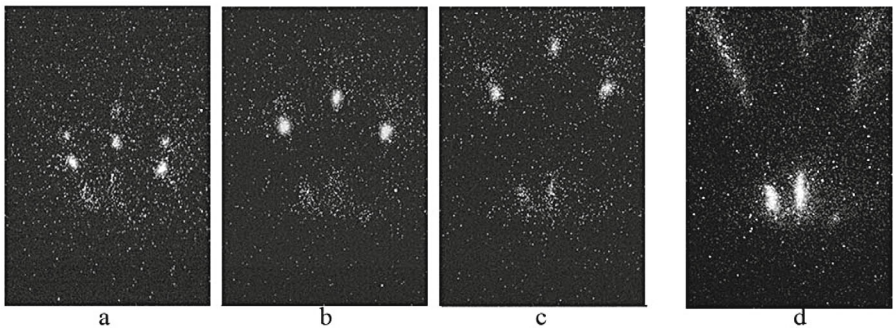

Fig. 8. Apokamp dynamics for three jets captured at an exposure of 3 ns and frame interval of 17 ns (a)–(c) and integral image at an exposure of 120 ns (d). The vertical frame size is 26.27 mm.

lower than that for APPJs in air [39]. Apparently, this feature distinguishes apokamps from plasma jets formed in a barrier discharge. It should also be noted that at these values of v, the contribution of convection to apokamps within the first 100 ns is negligible.

Additionally, we recorded the region directly between the electrodes (Fig. 9). The bright zones in the lower part of each image correspond to the sharp ends of the electrodes and glow about the same as the region from which the apokamp develops.

The temperature of these zones can be judged if we convert the images to colored ones as follows. Let us introduce a certain number of color grades i (in our case, $i = 11$) and assign equal image intensity intervals to each of the grade: $\delta = (I_{\max} - I_{\min})/i$. Then, to the ith grade there corresponds a range of pixel intensity $[I_{\min}+\delta\cdot(i-1); I_{\min}+\delta\cdot i]$. Given the ambient temperature for which $i = 0$, we can indirectly judge the temperature of zones differing in color. Thus, we can convert the initial image to a colored one. Such an image is shown in Figure 10. It is seen that the electrodes and the zones from which plasma jets develop are close in temperature, suggesting close current densities through the regions. It should be noted that long exposure times, e.g., hundred milliseconds typical of digital cameras, are inapplicable for the analysis because the plasma jets during this time can repeatedly change their positions and the entire observation zone can be blurred. At an exposure of ∼150–200 ns, this does not happen and one can accurately trace the location and temperature of near-electrode zones and plasma jets.

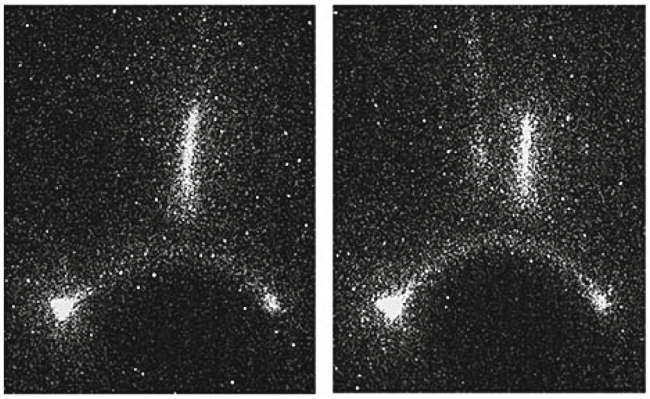

Fig. 9. Integral image of a single apokamp (at the left) and double apokamp (at the right). The exposure is 240 ns; the vertical frame size is 26.27 mm.

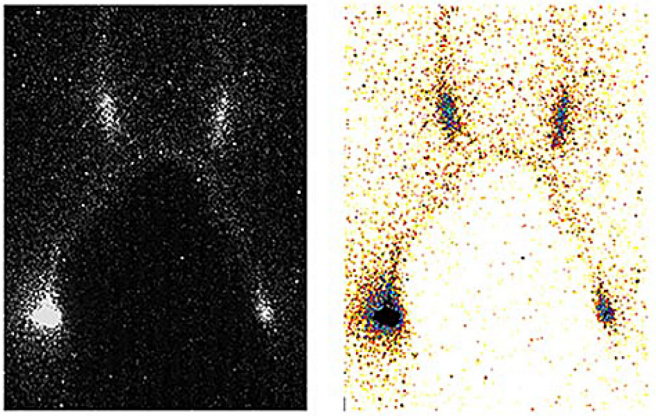

Fig. 10. Integral image of a double apokamp (at the left) and its color map (at the right). The exposure is 240 ns; the vertical frame size is 26.27 mm.

Our study suggests at least two mechanisms for the formation of apokamps: the propagation of streamers [1,34] and the effect of runaway electrons on the dynamics of ionization processes [46,47].

4 Conclusion

Thus, the research data demonstrate the following features of apokamps. The apokamp is always attached to the bending point of the current channel. Its formation does not depend on the shape and material of electrodes but depends strongly on the voltage amplitude. The apokamp length can reach 4–6 cm. The apokamp jet develops as plasma bullets moving with a velocity of 100–220 km/s and their propagation is little affected by convection. The phenomenon is observed in a narrow range of parameters, in particular in the vicinity of the maximum gap voltage. We can suggest two probable apokamp mechanisms: the propagation of streamers and the initiation of ionization waves by runaway electrons.

The authors are grateful to M.V. Andreev from the Institute of High Current Electronics SB RAS for help with data processing. The work is supported by the Russian Science Foundation (Project No. 14-29-00052).

References

1. X. Lu, G.V. Naidis, M. Laroussi, S. Reuter, D.B. Graves, K. Ostrikov, Phys. Rep. **630**, 1 (2016)
2. O.V. Penkov, M. Khadem, W.-S. Lim, D.-E. Kim, J. Coat. Technol. Res. **12**, 225 (2015)
3. J. Ehlbeck, U. Schnabel, M. Polak, J. Winter, Th. von Woedtke, R. Brandenburg, T. von dem Hagen, K.-D. Weltmann, J. Phys. D: Appl. Phys. **44**, 013002 (2011)
4. M.G. Kong, G. Kroesen, G. Morfill, T. Nosenko, T. Shimizu, J. van Dijk, J.L. Zimmermann, New J. Phys. **11**, 115012 (2009)
5. A. Schutze, J.Y. Jeong, S.E. Babayan, J. Park, G.S. Selwyn, R.F. Hicks, IEEE Trans. Plasma Sci. **26**, 1685 (1998)
6. Z. Machala, K. Hensel, Yu. Akishev, *Plasma for Bio-Decontamination, Medicine and Food Security*, NATO Science for Peace and Security Series A: Chemistry and Biology (Springer, 2012)
7. J. Tang, S. Li, W. Zhao, Y. Wang, Y. Duan, Appl. Phys. Lett. **100**, 253505 (2012)
8. O.S. Zhdanova, V.S. Kuznetsov, V.A. Panarin, V.S. Skakun, E.A Sosnin, V.F. Tarasenko, Prikl. Fiz. (Appl. Phys.) **2**, 34 (2015) (in Russian)
9. J.Y. Kim, J. Ballato, S.-O. Kim, Plasma Process. Polym. **9**, 253 (2012)
10. J.Y. Kim, D.-H. Lee, J. Ballato, W. Cao, S.-O. Kim, Appl. Phys. Lett. **101**, 224101 (2012)
11. A. Sarani, A.Y. Nikiforov, C. Leys, Phys. Plasmas **17**, 063504 (2010)
12. C. Cheng, S. Jie, X. De-Zhi, X. Hong-Bing, L. Yan, F. Shi-Dong, M. Yue-Dong, C. Paul K, Chin. Phys. B **23**, 075204 (2014)
13. A.S. Chiper, W. Chen, O. Mejlholm, P. Dalgaard, E. Stamate, Plasma Sources Sci. Technol. **20**, 025008 (2011)
14. K. Malecha, Sens. Actuators B **181**, 486 (2013)
15. S.E. Babayan, J.Y. Jeong, V.J. Tu, J. Park, G.S. Selwyn, R.F. Hicks, Plasma Source Sci. Technol. **7**, 286 (1998)
16. E. Stoffels, A.J. Flikweert, W.W. Stoffels, G.M.W. Kroesen, Plasma Sources Sci. Technol. **11**, 383 (2002)
17. J.R. Roth, D.M. Sherman, R.B. Gadri, F. Karakaya, Zhiyu Chen, T.C. Montie, K. Kelly-Wintenberg, P.P.-Y. Tsai, IEEE Trans. Plasma Sci. **28**, 56 (2000)
18. Ju.S. Akishev, M.E. Grushin, N.I. Trushkin, Patent RU 2398589, priority date 26.10.2007
19. X.L. Deng, A.Yu. Nikiforov, P. Vanraes, Ch. Leys, J. Appl. Phys. **113**, 023305 (2013)
20. G. Uchida, K. Takenaka, Y. Setsuhara, J. Appl. Phys. **117**, 153301 (2015)
21. K.L. Lai, K.K. Jayapalan, O.H. Chin, P.F. Lee, C.S. Wong, AIP Conf. Proc. **1657**, 150002 (2015)
22. T. Shao, C. Zhang, R. Wang, Y. Zhou, Q. Xie, Z. Fang, IEEE Trans. Plasma Sci. **43**, 726 (2015)
23. E.A. Sosnin, V.A. Panarin, V.S. Skakun, V.F. Tarasenko, D.S. Pechenitsin, D.S. Kuznetsov, Proc. SPIE **9810**, 98101I (2015)

24. E.A. Sosnin, V.A. Panarin, V.S. Skakun, V.F. Tarasenko, D.S. Pechenitsin, V.S. Kuznetsov, Tech. Phys. **61**, 789 (2016)
25. A. Abahazem, A. Mraihi, N. Merbahi, M. Yousfi, O. Eichwald, IEEE Trans. Plasma Sci. **39**, 2230 (2011)
26. X. Pei, X. Lu, J. Liu, D. Liu, Y. Yang, K. Ostrikov, P.K. Chu, Y. Pan, J. Phys. D: Appl. Phys. **45**, 165205 (2012)
27. Y.Ch. Hong, H.S. Uhm, Appl. Phys. Lett. **89**, 221504 (2006)
28. A.-A.H. Mohamed, J.F. Kolb, K.H. Shoenbach, Eur. Phys. J. D **60**, 517 (2010)
29. X. Li, J. Tang, X. Zhan, X. Yuan, Zh. Zhao, Y. Yan, Y. Duan, Appl. Phys. Lett. **103**, 033519 (2013)
30. Z. Niu, T. Shao, IEEE Trans. Plasma Sci. **39**, 2127495 (2011)
31. E.A. Sosnin, V.S. Skakun, V.A. Panarin, D.S. Pechenitsin, V.F. Tarasenko, E.Kh. Baksht, J. Exp. Theor. Phys. Lett. **103**, 761 (2016)
32. M. Teschke, J. Kedzierski, E.G. Finantu-Dinu, D. Korzec, J. Engemann, IEEE Trans. Plasma Sci. **33**, 310 (2005)
33. X. Lu, M. Laroussi, J. Appl. Phys. **100**, 063302 (2006)
34. G.V. Naidis, J. Phys. D: Appl. Phys. **43**, 402001 (2010)
35. E. Karakas, M. Laroussi, J. Appl. Phys. **108**, 063305 (2010)
36. X. Lu, M. Laroussi, V. Puech, Plasma Sources Sci. Technol. **21**, 034005 (2012)
37. Y.B. Xian, P. Zhang, X.P. Lu, X.K. Pei, S.Q. Wu, Q. Xiong, K. Ostrikov, Sci. Rep. **3**, 1599 (2013)
38. S. Wu, X. Lu, Phys. Plasmas **21**, 123509 (2014)
39. D.A. Lacoste, A. Bourdon, K. Kuribara, K. Urabe, S. Stauss, K. Terashima, Plasma Sources Sci. Technol. **23**, 062006 (2014)
40. S. Wu, H. Xu, Y. Xian, Y. Lu, X. Lu, AIP Adv. **5**, 027110 (2015)
41. Y.B. Xian, X.P. Lu, S.Q. Wu, P.K. Chu, Y. Pan, Appl. Phys. Lett. **100**, 123702 (2012)
42. M.F. Zhukov, A.S. Koroteev, B.A. Uryukov, *Applied Dynamics of Thermal Plasma* (Nauka, Novosibirsk, 1975) (in Russian)
43. E.A. Sosnin, V.S. Skakun, V.A. Panarin, V.F. Tarasenko, O.S. Zhdanova, P.A. Goltsova, Modern Sci. Res. Innov. (2016), URL: http://web.snauka.ru/en/issues/2016/03/65016
44. J. Mahoney, W. Zhu, V.S. Johnson, K.H. Becker, J.L. Lopez, Eur. Phys. J. D **60**, 441 (2010)
45. J. Shi, F. Zhong, J. Zhang, D.W. Liu, M.G. Kong, Phys. Plasmas **15**, 013504 (2008)
46. M.I. Lomaev, D.V. Beloplotov, V.F. Tarasenko, D.A. Sorokin, IEEE Trans. Dielectr. Electr. Insul. **22**, 1833 (2015)
47. V.F. Tarasenko, D.V. Beloplotov, M.I. Lomaev, Plasma Phys. Rep. **41**, 832 (2015)